A 1550-nm linearly tunable continuous wave single-mode external cavity diode laser based on a single-cavity all-dielectric thin-film Fabry–Pérot filter*

Xiao Xiao(肖 啸), Lu Yuan-Fu(鲁远甫), Yu Feng-Qi(于峰崎)†, and Jin Lei(金 雷)

Shenzhen Institutes of Advanced Technology, Chinese Academy of Sciences, Shenzhen 518055, *China*
Chinese University of Hong Kong, Hong Kong, China

(Received 12 October 2012; revised manuscript received 1 December 2012)

A 1550-nm linearly tunable continuous wave (CW) single-mode external cavity diode laser (ECDL) based on a single-cavity all-dielectric thin-film Fabry–Pérot filter (s-AFPF) is proposed and realized in this paper. Its internal optical components as well as their operation mechanisms are introduced first, and then its longitudinal mode output characteristic is theoretically analyzed. Afterwards, we set up the experimental platform for the output characteristic measurement of this tunable ECDL; under different experimental conditions, we execute accurate and real-time measurements for the output central wavelength, output optical power, output longitudinal mode distribution, and the line-width of the tunable ECDL in its tuning process. By summing up the optimal experimental condition from the measured data, we obtain the optimal tunable ECDL relevant parameters: the tunable ECDL has a linear mode-hop-free wavelength tuning region of 1547.203 nm–1552.426 nm, a stable output optical power in the range of 40 μW–50 μW, and a stable output longitudinal mode distribution of a single longitudinal mode with a line-width in the range of 100 MHz–150 MHz. This tunable ECDL can be used in environmental gas monitoring, atomic and molecular laser spectroscopy research, precise measurements, and so on.

Keywords: thin-film optical properties, tunable external cavity diode laser, laser spectroscopy

PACS: 78.66.–w, 42.55.Px, 42.62.Fi, 42.60.Fc **DOI:** 10.1088/1674-1056/22/7/077802

1. Introduction

Tunable external cavity diode lasers (ECDLs) are playing an increasingly important role in coherent optical telecommunications, atomic and molecular laser spectroscopy, precise measurements, and environmental monitors.[1] Currently, two principal configurations in tunable ECDLs are the Littrow configuration[2–7] and the Littman–Metcalf configuration,[8–11] and in both the dispersive element is a bulk diffraction grating. Besides, there are also other external cavity configurations which contain different kinds of dispersive elements such as Fabry–Pérot etalons,[12,13] acousto–optic filters,[14,15] electro–optic filters,[16,17] and others.

The tunable ECDL based on Fabry–Pérot etalon, however, is not as popular as either the Littrow configuration or the Littman–Metcalf configuration. A considerable reason is that the performance of the early air-spaced etalons was not good enough, and in a tunable ECDL, it is hard for the air-spaced etalon to have a simple but effective tuning mechanism which can make one of its pass-band center wavelengths have a synchronous variation with a certain fixed external cavity longitudinal mode wavelength. With the development of thin-film optics, the air-spaced etalon can be replaced with a high-performance solid etalon which is manufactured with thin-film coating technology, so as to improve the performance and popularity of Fabry–Pérot etalon based tunable ECDL.

In this paper, we propose a 1550-nm linearly tunable continuous wave (CW) single-mode ECDL based on a single-cavity all-dielectric thin-film Fabry–Pérot filter (s-AFPF),[18–25] which is exactly a high-performance solid etalon fabricated with thin-film coating technology. Compared with the air-spaced etalon, the s-AFPF has a large value in its optical intensity transmission band (namely pass band) full-width at half-maximum (FWHM); but for the s-AFPF, there is only one pass band in a fairly wide-wavelength band range around 1550 nm, which is different from that for the air-spaced etalon. This tunable ECDL adopts a novel external cavity tuning mechanism to achieve a synchronous variation between the pass-band center wavelength of its dispersive element s-AFPF and its certain fixed external cavity longitudinal mode wavelength; its schematic configuration is shown in Fig. 1. By theoretical and experimental demonstrations, we show that the tunable ECDL possesses a linear mode-hop-free wavelength tuning region of 1547.203 nm–1552.426 nm, which covers a 5-nm range centered at about 1550 nm.

*Project supported by the Key Laboratory of Functional Crystals and Laser Technology, Chinese Academy of Sciences (Grant No. JTJG201109), the Guangdong Province & Chinese Academy of Sciences Comprehensive Strategic Cooperation Project (Grant No. 2010A090100014), and the 2009 Technology Research and Development Fund of Shenzhen, China (Grant No. O702011001).

†Corresponding author. E-mail: fq.yu@siat.ac.cn

© 2013 Chinese Physical Society and IOP Publishing Ltd

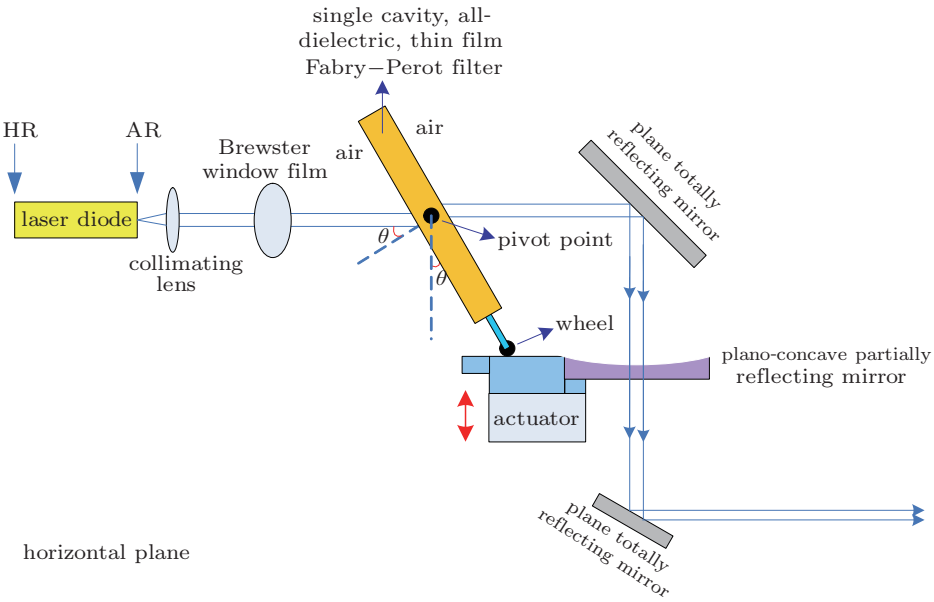


Fig. 1. (color online) An external cavity configuration to maintain a single longitudinal mode as the s-AFPF is rotated. A single actuator acts to i) move the partially reflecting mirror that forms one end of the external cavity and ii) rotate the s-AFPF around its pivot point. If the actuator is moved forward, the cavity shortens and the wavelength of a given longitudinal mode decreases in a linear manner. At the same time, the incident angle at s-AFPF(θ) is increased by the actuator pushing against the wheel. The larger incident angle moves the pass-band center wavelength of s-AFPF to a smaller value with a quasi-linear dependence on the cosine of θ. For a proper set of design parameters, the wavelength of a given longitudinal mode and the wavelength of the pass-band center of s-AFPF may be made to track each other fairly well over a significant range of actuator motion, leading to mode-hop-free performance.

2. Characteristics of an s-AFPF

The membrane structure of an s-AFPF is shown in Fig. 2, and it consists of one spacer layer and two symmetrical reflectors. The spacer layer is a half-wave layer, and the two symmetrical reflectors are composed of alternate quarter-wave layers. The detailed membrane structure of an s-AFPF can be divided into two types according to its spacer layer: $(HL)^P$H–2L–H$(LH)^P$ or $(HL)^P$–2H–$(LH)^P$ as indicated in Fig. 3. The capital "H" represents a high-index dielectric medium and the capital "L" denotes a low-index dielectric medium, both with an optical thickness of a quarter-wave. From Fig. 3, we can see the "H" layer and "L" layer alternate anywhere except in the spacer layer. In the spacer layer, the medium consists of either two "H" layers or two "L" layers.[18] We use the term "*P*-value" to indicate exponent *P*. In an actual fabrication process, the membrane structure of as s-AFPF is usually deposited on a substrate, which is some type of glass. On the opposite side of the substrate, anti-reflective (AR) coating is deposited to prevent multi-beam interference from occurring in the substrate. Therefore, the actual design structure of an s-AFPF is either Air$|(HL)^P$H–2L–H$(LH)^P|$Glass or Air$|(HL)^P$–2H–$(LH)^P|$Glass.

For the investigation in this paper, we assume that the design structure of the s-AFPF is Air$|(HL)^P$H–2L–H$(LH)^P|$Glass, in which the "H" layer is the high-index dielectric medium Ta_2O_5 with a refractive index of 2.06, the "L" layer is the low-index dielectric medium SiO_2 with a refractive index of 1.46, and the "Glass" is the substrate medium K9 glass with a refractive index of 1.5168. We do not consider the dispersion of any refractive material, because of the relatively small wavelength band and the low dispersion for these refractive materials around 1550 nm. We also assume that the physical thicknesses of "H" layer, "L" layer, and "Glass" substrate are 193.57 nm, 273.12 nm, and 2 mm, respectively; the "*P*-value" in Air$|(HL)^P$H–2L–H$(LH)^P|$Glass is 7. Considering the configuration in Fig. 4, an incident plane wave at the s-AFPF mentioned above with incident angle of θ is shown. When the s-AFPF rotates around a pivot point, θ will change continuously.

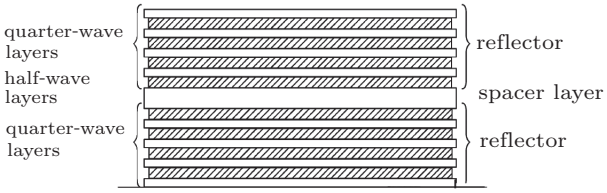


Fig. 2. Membrane structure of an s-AFPF.

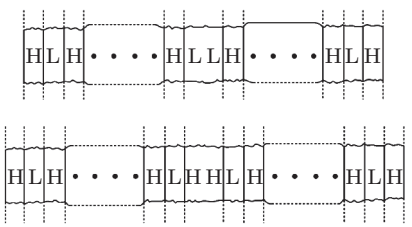


Fig. 3. Two basic types of an s-AFPF.

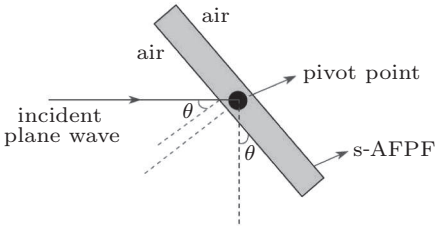


Fig. 4. An incident plane wave at an s-AFPF with a continuously changing incident angle of θ when the s-AFPF rotates around a pivot point.

By using the characteristic matrix method,[18] we theoretically analyze the transmission performance of the s-AFPF mentioned above for the TE and TM plane waves at four different incident angles[26] as indicated in Fig. 5. At an incident angle of 0°, there are two identical extremely narrow transmission bands of the s-AFPF for the TE and TM plane waves; as the incident angle θ increases from 0° to 36°, the TE and TM curves separate off gradually, both of which will move to the short-wavelength region, but only the TE plane wave transmission band has a faster movement speed. We can control the shift of transmission-band center for either a TE or a TM plane wave by rotating the s-AFPF around a pivot point.

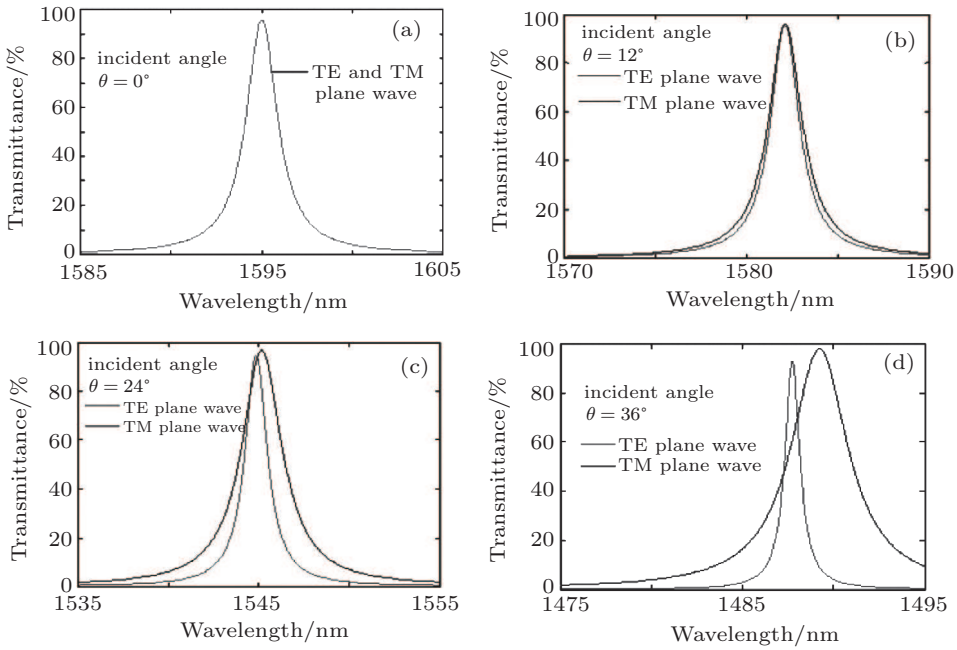


Fig. 5. Simulated "transmittance-wavelength" curves of s-AFPF Air|$(HL)^7$H–2L–H$(LH)^7$|Glass mentioned above penetrated by TE and TM plane waves at four different incident angles: (a) $\theta = 0°$, (b) $\theta = 12°$, (c) $\theta = 24°$, (d) $\theta = 36°$.

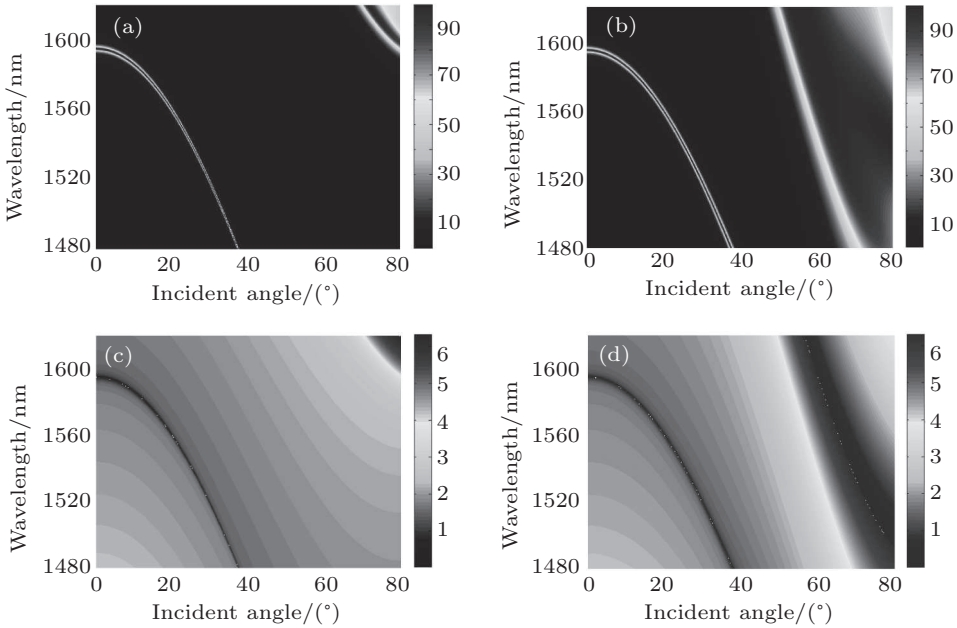


Fig. 6. Distributions of optical intensity transmittance and phase variation as a function of wavelength versus incident angle for TE and TM plane waves, as they pass through the s-AFPF Air|$(HL)^7$H–2L–H$(LH)^7$|Glass. (a) Optical intensity transmittance (in %) for the TE plane wave, (b) Optical intensity transmittance (in %) for the TM plane wave, (c) phase variation (in radian) for the TE plane wave, (d) phase variation (in radian) for the TM plane wave.

Figure 6 presents the distributions of optical intensity transmittance and phase variation as a function of wavelength versus incident angle for TE and TM plane waves, as they pass through Air|$(HL)^7H$–2L–$H(LH)^7$|Glass. The optical intensity peak-transmittance wavelength follows a quasi-parabolic curve versus incident angle. Figure 7 shows the relationship between optical intensity peak-transmittance wavelength and the cosine value of the incident angle for TE and TM plane waves. We note that the optical intensity peak-transmittance wavelength follows a quasi-linear curve versus the cosine value of the incident angle for both TE and TM plane waves. This quasi-linear property with respect to the cosine value of the incident angle suggests to us a configuration that might have special advantages.

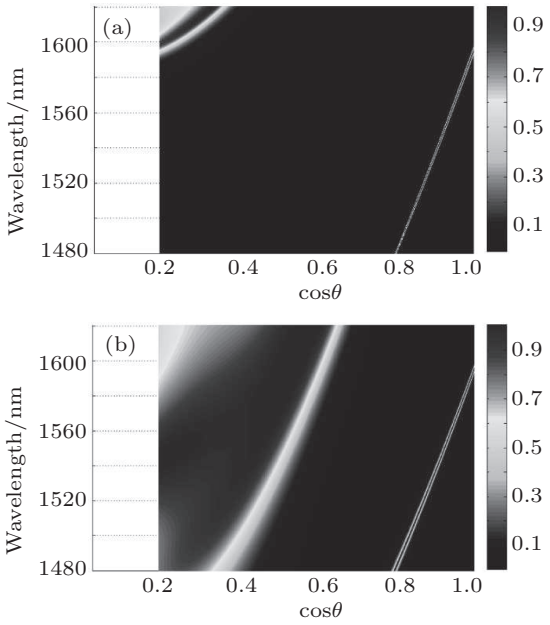


Fig. 7. Distributions of optical intensity transmittance as a function of wavelength versus the cosine value of the incident angle for (a) TE and (b) TM plane waves, as they pass through the s-AFPF Air|$(HL)^7$H-2L-$H(LH)^7$|Glass.

3. Internal structure of the tunable ECDL

In Fig. 1, a circular s-AFPF simulated above with a diameter of 20 mm is inserted into the ECDL external cavity; the s-AFPF is vertical to the horizontal plane, but not vertical to the optical axis; it can self-rotate around its central pivot point. The light source in this tunable ECDL is a special laser diode called reflective semiconductor optical amplifier (RSOA, IPSAD1501-3500); on its one side, a high-reflective (HR) thin-film coating with a reflectivity of about 90% is deposited; on its other side, an AR thin-film coating with a reflectivity less than 0.01% is deposited; the RSOA light is emitted from its AR coated side, and the collimating lens is also AR coated; the central wavelength of the RSOA light is 1550 nm, and its 3-dB bandwidth is 60 nm; the small signal gain at peak wavelength of the RSOA is 25 dB, and the threshold current of the RSOA is 15 mA; the output power of the RSOA is typically 2 mW, and its polarization dependent gain is 12 dB; the operation temperature of the RSOA is always maintained at 25° by a thermoelectric cooler (TEC). As the polarization dependent gain of the RSOA is 12 dB, its output is mainly TE polarized light (vertical to the horizontal plane), as well as a small amount of TM polarized light (parallel to the horizontal plane). To ensure that the output of the tunable ECDL is purely TE polarized light, we insert a circular Brewster window film into the ECDL external cavity, so as to let TE polarized light pass through and TM polarized light be reflected away by it. The Brewster window film is made of K9 glass without thin-film coating; it has a diameter of 20 mm and a physical thickness of 2 mm; the intersecting line between the Brewster window film plane and the horizontal plane is vertical to the optical axis; the Brewster window film plane has a 33.4° with respect to the horizontal plane, which can make the RSOA light beam irradiate on the window film at the incident angle of Brewster angle (56.6°). There are two identical circular plane totally reflecting mirrors in the configuration of the tunable ECDL; their reflectivity values are both 100% when the RSOA light beam irradiates on them at an incident angle of 45°. There is also a circular Plano-concave partially reflecting mirror positioned in the tunable ECDL configuration, and it is vertical to the optical axis; it is made of K9 glass, and has a diameter of 25.4 mm; the curvature radius of its concave surface is 500 mm; a partially-reflective (PR) thin-film coating is deposited on its concave surface while an AR coating is deposited on its plane surface.

Thus, the HR coated side of the RSOA and the concave surface of the Plano-concave partially reflecting mirror form a resonator of the tunable ECDL. According to the principle of laser resonator, the external cavity longitudinal mode wavelength changes linearly with optical path length, becoming shorter with optical path length decreasing. However, with the increase of cavity length, the free spectral range (FSR) of the longitudinal modes decreases, so a long ECDL has a high spectral density of modes. Many longitudinal modes appearing under the gain width will lead to multi-longitudinal mode output or the laser hopping between modes, creating an undesirable performance. In order to filter out the unwanted longitudinal modes, we insert an s-AFPF discussed above into the external cavity and use its narrow spectral band to reject all modes except for the single desired longitudinal mode.

Meantime, for the TE polarized light, Fig. 7 shows that the optical intensity peak-transmittance wavelength of the s-AFPF also changes in a quasi-linear manner such that the wavelength decreases linearly with $\cos\theta$ increasing (θ is the TE wave incident angle at s-AFPF) in a certain wavelength range around 1550 nm. Hence, if the optical path length and $\cos\theta$ can both decrease simultaneously, and by a proper de-

sign of configuration, these two effects may be made to compensate for each other to create a substantial mode-hop-free spectral band.

In Fig. 1, the tunable ECDL configuration uses a single actuator to control both the external cavity length and the light beam incident angle at the s-AFPF. We assume that the initial position of the actuator is where the light beam incident angle at s-AFPF is zero. For forward movement of the actuator from the initial position, the external cavity length decreases and the wavelength of a single longitudinal mode shortens in a linear manner. Meantime, as the actuator pushes forward against the wheel, it drives the s-AFPF to self-rotate counter clock-wise around the pivot point, so as to drive the light beam incident angle at s-AFPF to larger values and the cosine of angle to smaller values, and to make the optical intensity peak-transmittance wavelength of s-AFPF decrease in a quasi-linear manner.

For simplicity, we regard the collimated laser beam in Fig. 1 as a plane wave. Then, the incident light wave at s-AFPF is now a TE plane wave. For a TE plane wave, we need to consider whether there is a synchronous variation between the pass-band center wavelength of the dispersive element s-AFPF and a certain fixed external cavity longitudinal mode wavelength in the process of actuator translation from its initial position.

If we calculate the fractional (longitudinal) mode number [see Eq. (1)] of the pass-band center wavelength of the s-AFPF in the process of actuator translation, we can find which external cavity longitudinal mode will have a synchronous wavelength variation with the s-AFPF pass-band center wavelength. We assume that the initial position of the actuator is where the light beam incident angle at s-AFPF is zero. For forward movement of the actuator from the initial position, the decrease in both the external cavity optical path length and $\cos\theta$ will appear simultaneously, and there is a linear variation relationship between them. If the length from the pivot point center to the wheel center is set properly for the s-AFPF discussed above, the optical intensity peak-transmittance wavelength of the s-AFPF and the wavelength of a certain fixed external cavity longitudinal mode may be made to match rather well over a significant range, thereby achieving a linear mode-hop-free wavelength tuning performance. Let the actuator displacement from the initial position be x, the physical thickness of the s-AFPF substrate be h, the refractive index of the s-AFPF substrate be n, the length from the pivot point center to the wheel center be L. In the meantime, let the optical intensity peak-transmittance wavelength of the s-AFPF for TE polarized light be $\lambda_s(x)$, the round trip optical path length of external cavity be $L_{OP}(x)$. We define a fractional mode number of $\lambda_s(x)$, $m_s(x)$, which is the ratio of $L_{OP}(x)$ to $\lambda_s(x)$ as

$$m_s(x) = \frac{L_{OP}(x)}{\lambda_s(x)}. \tag{1}$$

The fractional mode number $m_s(x)$ is simply a real number, which refers to the mode number at which the mode should be for maximum s-AFPF transmission. If $L_{OP}(x)$ is made to track $\lambda_s(x)$ closely as x varies, $m_s(x)$ will be nearly constant and an ECDL running on $\lambda_s(x)$ may be mode-hop-free over a relatively wide range.

Figure 8 shows the details that affect the round trip optical path length of external cavity as the actuator pushes forward from its initial position. In Fig. 8, let the external cavity optical path difference between the initial position P_1 and the current position P_2 be D_{OP}, then we will have

$$D_{OP} = 2\left[(a+nh+b_1+b_2) - \left(a-h_1+\frac{nh}{\cos\alpha}+y_1+y_2\right)\right]. \tag{2}$$

We also have

$$a+h+b_1+b_2-x = (a-h_1)+\frac{h\cos(\theta-\alpha)}{\cos\alpha}+y_1+y_2. \tag{3}$$

we substitute Eq. (3) into Eq. (2) to eliminate y_1+y_2 and then obtain

$$D_{OP} = 2\left[nh-\frac{nh}{\cos\alpha}-h+x+\frac{h\cos(\theta-\alpha)}{\cos\alpha}\right]. \tag{4}$$

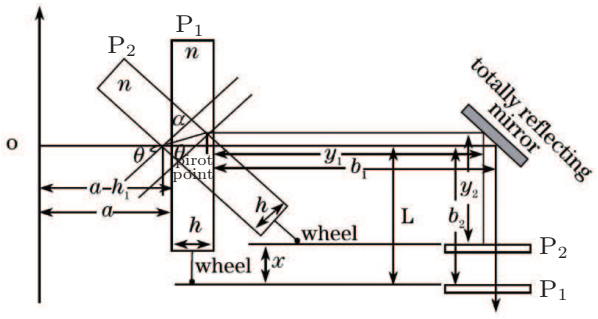


Fig. 8. Schematic diagram of how external cavity optical path varies as the actuator pushes forward from its initial position. Note that the s-AFPF rotates as the wheel is also pushed forward. The length from the pivot point center to the wheel center is L. The angle of rotation θ is determined by both x and L according to Eq. (6) and it is set to be the value corresponding to the wavelength of maximum transmission of the s-AFPF.

From Fig. 8, we know

$$\cos\alpha = \sqrt{1-(\sin\alpha)^2} = \sqrt{1-\left(\frac{\sin\theta}{n}\right)^2} = \frac{\sqrt{n^2-1+\cos^2\theta}}{n}, \tag{5}$$

$$\cos\theta = \frac{L-x}{L}. \tag{6}$$

Hence, we have

$$\cos\alpha = \frac{\sqrt{n^2L^2+x^2-2xL}}{nL}, \tag{7}$$

$$\cos(\theta-\alpha)=\frac{2xL-x^2+(L-x)\sqrt{n^2L^2+x^2-2xL}}{nL^2}. \quad (8)$$

We substitute Eqs. (7) and (8) into Eq. (4) to obtain the change in external cavity round trip optical path length, $D_{\mathrm{OP}}(x)$ expressed as follows:

$$D_{\mathrm{OP}}(x) = 2\left[nh-\frac{n^2hL}{\sqrt{n^2L^2+x^2-2xL}}-h+x + \frac{2xhL-x^2h+h(L-x)\sqrt{n^2L^2+x^2-2xL}}{L\sqrt{n^2L^2+x^2-2xL}}\right]. \quad (9)$$

In Eq. (9), once the parameters of the laser structure are finalized, n, h, and L will be constant, only x is a variable. Therefore, Eq. (1) can further be written as

$$m_{\mathrm{s}}(x)=\frac{L_{\mathrm{OP}}(x)}{\lambda_{\mathrm{s}}(x)}=\frac{L_{\mathrm{OP}}(0)-D_{\mathrm{OP}}(x)}{\lambda_{\mathrm{s}}(x)}. \quad (10)$$

In the tunable ECDL discussed above, we set L to be 81 mm, and the round trip optical path length of the external cavity at initial position $L_{\mathrm{OP}}(0)$ to be 449.9 mm. Then, by a theoretical calculation, as the actuator pushes forward from its initial position, $m_{\mathrm{s}}(x)$ will first increase and then decrease, as shown in Fig. 9. In Fig. 9, the relationship curve between $m_{\mathrm{s}}(x)$ and $\lambda_{\mathrm{s}}(x)$ is given, as the incident angle of TE wave at s-AFPF varies from 0° to 37°; there is only a limited flat region at the top of the curve, in which the fractional longitudinal mode number can keep unchanged. It shows that only in this flat region, can the optical intensity peak-transmittance wavelength of the s-AFPF for TE polarized light have a synchronous variation with the wavelength of a certain fixed external cavity longitudinal mode, and this region is thus called the mode-hop-free wavelength tuning region. Theoretically, the mode-hop-free wavelength tuning region covers a range of 1547.3 nm–1552.6 nm, the corresponding actuator displacement from the initial position is 5.9 mm–6.7 mm, and the locked and output external cavity longitudinal mode numbers are 282 and 254 respectively.

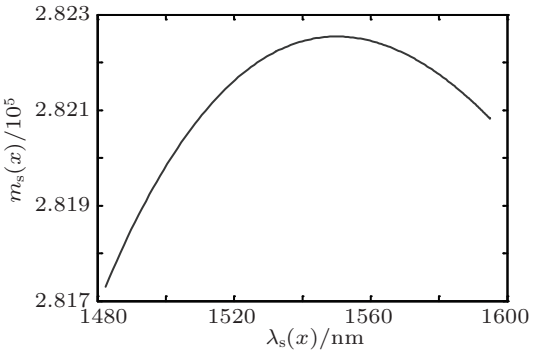


Fig. 9. Relationship curve between the pass-band center wavelength of s-AFPF $\lambda_{\mathrm{s}}(x)$ and its corresponding fractional mode number $m_{\mathrm{s}}(x)$ from Eq. (10), as the TE wave incident angle at s-AFPF varies from 0° to 37°. The peak of the curve centerd approximately at 1551.5 nm, has a mode-hop-free wavelength range of about 8 nm. The central wavelength of the widest mode-hop-free range can be selected by setting the pivot-to-wheel length L. Here, $L=81$ mm, and $L_{\mathrm{OP}}(0)=449.9$ mm.

4. Output characteristic measurement of the tunable ECDL

The output characteristic measurement of the tunable ECDL refers to the measurements of its output central wavelength, output optical power, output longitudinal mode distribution, and line-width.

The schematic diagram for the output central wavelength and output optical power measurement of the tunable ECDL is shown in Fig. 10(a). In Fig. 10(a), the optical components in the tunable ECDL have been introduced in Fig. 1. Besides, we use a plane partially reflecting mirror to split the output laser beam of the tunable ECDL into two parts: one is first reflected by a plane totally reflecting mirror group and then enters into an optical spectrum analyzer (OSA) – the VERTEX 80v vacuum FT-IR spectrometer; the other is first reflected by a plane totally reflecting mirror and then enters into a laser power meter (LPM) probe. The reflectivity of that plane partially reflecting mirror approaches to 90% when the light beam around 1550 nm irradiates on it at an incident angle of 45°. The OSA is made by the BRUKER Corporation in Germany, and it is used to measure the tunable ECDL output central wavelength. The LPM is made by the OPHIR Corporation in Israel, and it is used to measure the tunable ECDL output optical power; it consists of a laser power meter NOVA II and a laser power probe PD300-IR. The laser power probe PD300-IR has a germanium detector, an aperture of φ5 mm, a power range from 30 mW to 5 nW versus 300 mW to 200 μW, and a resolution of 0.01 nanowatts.

The schematic diagram for the output longitudinal mode distribution and line-width measurement of the tunable ECDL is shown in Fig. 10(b). In Fig. 10(b), the optical components in the tunable ECDL have been introduced in Fig. 1. Besides, we use a plane totally reflecting mirror to direct the output laser beam of the tunable ECDL into a convergent lens that has a focal length of 200 mm. After being focused by the convergent lens, the laser beam will enter into a scanning Fabry–Pérot interferometer (SFPI), and the focus of the convergent lens is generally located in the center of the SFPI cavity. The SFPI is made by the THORLABS Corporation in USA, and it is used to measure the tunable ECDL output longitudinal mode distribution and line-width; it consists of a scanning Fabry–Pérot interferometer SA200-12B and a scanning Fabry–Pérot controller box SA201.

Then, in the measurement of the tunable ECDL output characteristics, the room temperature is 25 °C while the relative humidity is 60% RH; the RSOA drive current is 230 mA; the reflectivity values of the PR coating on concave surface of the Plano-concave partially reflecting mirror can be 60%, 70%, 80%, and 90% for the RSOA light beam; other experimental conditions and parameters are the same as the ones mentioned before.

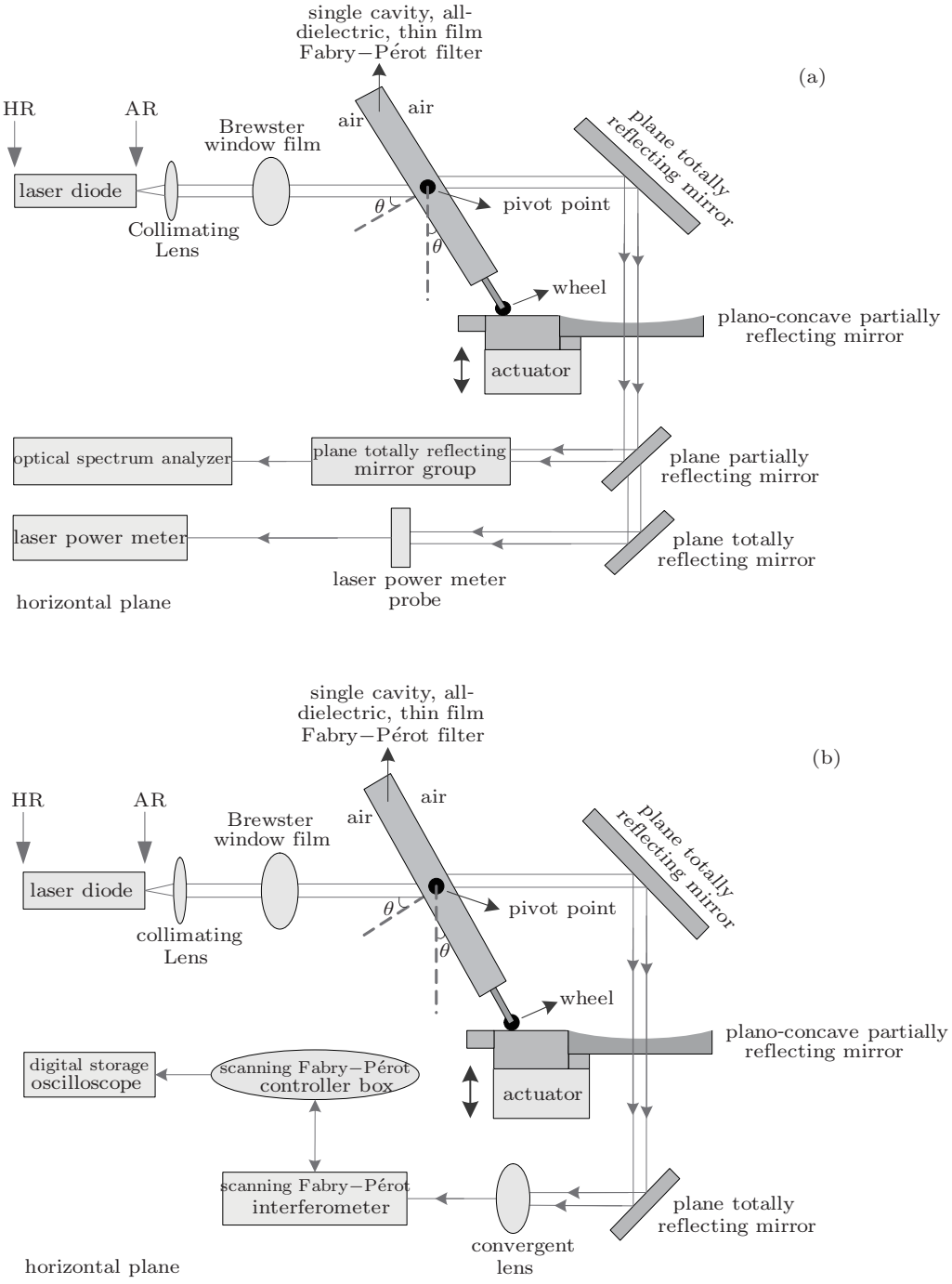


Fig. 10. Schematic diagram for the output characteristic measurement of the 1550 nm tunable ECDL based on an s-AFPF: panel (a) is for the measurement of output central wavelength versus output optical power of the 1550 nm tunable ECDL, and panel (b) for the measurement of output longitudinal mode distribution and line-width of the 1550 nm tunable ECDL.

As the actuator displacement from its initial position x varies, the actual output central wavelength λ and output optical power p of the tunable ECDL will also change. Let x vary from 5.9 mm to 6.7 mm, the varying step of x be 0.04 mm, and the PR coating reflectivity values of the Plano-concave partially reflecting mirror be 60%, 70%, 80%, and 90%, respectively, then we can draw the "λ–x" curve in Fig. 11(a) and the "p–x" curve in Fig. 11(c), from which we note that both the "λ–x" curve and the "p–x" curve will be dependent on PR coating reflectivity of the Plano-concave partially reflecting mirror.

As the value of x changes, the tunable ECDL output longitudinal mode distribution and line-width $\Delta\lambda$ are also changing. Let x vary from 5.9 mm to 6.7 mm, the varying step of x be 0.1 mm, and the PR coating reflectivity values of the Plano-concave partially reflecting mirror be 60%, 70%, 80%, and 90%, respectively, then we can draw the "$\Delta\lambda$–x" curve in Fig. 11(b), from which we note that the "$\Delta\lambda$–x" curve will be also dependent on PR coating reflectivity of the Plano-concave

partially reflecting mirror.

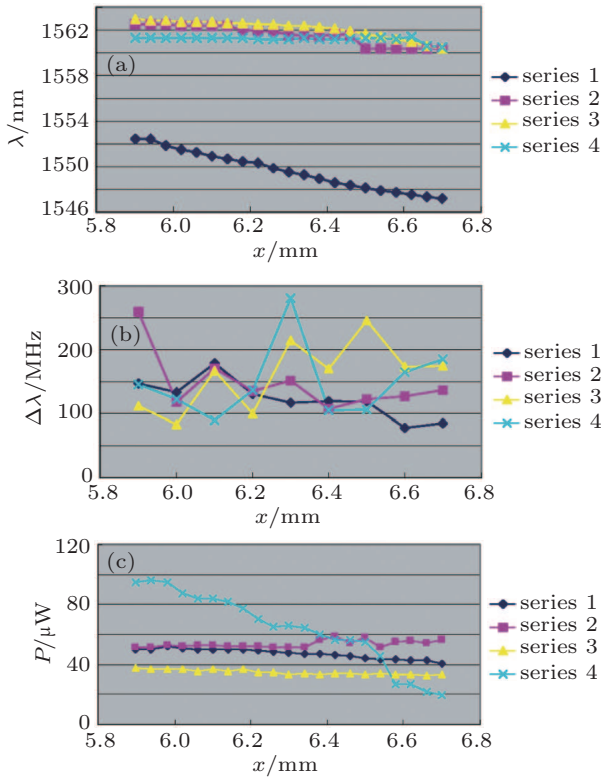


Fig. 11. (color online) Results of the tunable ECDL output characteristic measurement for the PR coating reflectivity values of 60%, 70%, 80%, and 90%, respectively. The room temperature is 25 °C, the relative humidity is 60% RH, and the RSOA drive current is 230 mA, as the actuator displacement from the initial position varies from 5.9 mm to 6.7 mm: panel (a) shows the output central wavelength λ; panel (b) displays the output longitudinal mode line-width $\Delta\lambda$; panel (c) presents the output optical power mm P. In panels (a), (b), and (c), series 1 corresponds to the PR coating reflectivity of 60%; series 2 corresponds to the PR coating reflectivity of 70%; series 3 corresponds to the PR coating reflectivity of 80%; series 4 corresponds to the PR coating reflectivity of 90%.

5. Conclusion

Compared with distributed feedback (DFB) laser, the proposed RSOA based tunable external cavity diode laser has an advantage of a narrow line-width. We measure the output characteristics of the proposed 1550-nm linearly tunable CW single-mode ECDL under different experimental conditions. When the RSOA drive current is 230 mA, the round trip optical path length of the external cavity at initial position is 449.9 mm, the actuator displacement from the initial position varies from 5.9 mm to 6.7 mm, and the PR coating reflectivity values of the Plano-concave partially reflecting mirror are 60%, 70%, 80%, and 90%, respectively, as can be seen from the measurement results in the previous section: i) for the PR coating reflectivity of 60%, when the actuator displacement from the initial position varies in a range of 5.9 mm–6.7 mm, the tunable ECDL will have a linear mode-hop-free wavelength tuning region of 1547.203 nm–1552.426 nm, which is consistent with the theoretical prediction. The tunable ECDL will also have a stable output optical power in the range of 40 μW–50 μW, and a stable output longitudinal mode distribution of a single longitudinal mode with a line-width in the range of 100 MHz∼150 MHz;[27] ii) for the PR coating reflectivity values of 70% and 80%, when the actuator displacement from the initial position varies in the range of 5.9 mm–6.7 mm, the tunable ECDL will have a stable output central wavelength in the range of 1560 nm–1563 nm, in which there is no significant linear change and the result is not consistent with the theoretical prediction. The tunable ECDL will also have a stable output optical power in the range of 50 μW–60 μW and 30 μW–40 μW, respectively. The tunable ECDL output longitudinal mode distribution is always of a single longitudinal mode, but the line-width has a large fluctuation and is not stable enough; iii) for the PR coating reflectivity of 90%, when the actuator displacement from the initial position varies in the range of 5.9 mm–6.7 mm, the tunable ECDL will have a stable output central wavelength in the range of 1560 nm∼1561 nm, in which there is no significant linear change and the result is not consistent with the theoretical prediction. The tunable ECDL will have an unstable output optical power in the range of 20 μW–100 μW. The tunable ECDL output longitudinal mode distribution is basically of a single longitudinal mode, but the line-width value is unstable.

In conclusion, when the PR coating reflectivity of the Plano-concave partially reflecting mirror is 60%, the output characteristics of the tunable ECDL will achieve the optimum. At this moment, the RSOA drive current is 230 mA, and the round trip optical path length of the external cavity at the initial position is 449.9 mm. The tunable ECDL will have a linear mode-hop-free wavelength tuning region of 1547.203 nm–1552.426 nm, a stable output optical power in the range of 40 μW–50 μW, and a stable output longitudinal mode distribution of a single longitudinal mode with a line-width in the range of 100 MHz–150 MHz, as the actuator displacement from the initial position varies from 5.9 mm to 6.7 mm. With these parameters, we can package and stereotype this tunable ECDL.

References

[1] Ye C Y 2004 *Tunable External Cavity Diode Lasers* (Singapore: World Scientific Press)
[2] de Labachelerie M and Passedat G 1993 *Appl. Opt.* **32** 269
[3] Bagley M, Wyatt R, Elton D J, Wickes H J, Spurdens P C, Seltzer C P, Cooper D M and Devlin W J 1990 *Electron. Lett.* **26** 267
[4] Tabuchi H and Ishikawa H 1990 *Electron. Lett.* **26** 742
[5] Favre F, le Guen D, Simon J C and Landousies B 1986 *Electron. Lett.* **22** 795
[6] Favre F and Le Guen D 1991 *Electron. Lett.* **27** 183
[7] Levin L 2002 *Opt. Lett.* **27** 231
[8] Liu K and Littman M G 1981 *Opt. Lett.* **6** 117
[9] Shoshan I, Danon N N and Oppenheim U P 1977 *J. Appl. Phys.* **48** 4495
[10] Littman M G and Metcalf H J 1978 *Appl. Opt.* **17** 2224
[11] McNicholl P and Metcalf H J 1985 *Appl. Opt.* **24** 2757

[12] Salathe R P 1979 *Appl. Phys.* **20** 1
[13] Boshier M G, Berkeland D, Hinds E A and Sandoghdar V 1991 *Opt. Commun.* **85** 355
[14] Hidaka T and Nakamoto T 1989 *Electron. Lett.* **25** 1320
[15] Coquin G A and Cheung K W 1988 *Electron. Lett.* **24** 599
[16] Andrews J R 1991 *Opt. Lett.* **16** 732
[17] Greiner G, Boggs B, Wang T and Mossberg T W 1998 *Opt. Lett.* **23** 1280
[18] Macleod H A 1999 *Thin-Film Optical Filters* (Lindon: Institute of Physics Press)
[19] Zorabedian P and Trutna Jr W R 1988 *Opt. Fiber Commun.* 1 WQ27
[20] Zorabedian P and Trutna Jr W R 1988 *Opt. Lett.* **13** 826
[21] Zorabedian P 2000 *U.S. Patent* **108** 355
[22] Svilans 2003 *U.S. Patent* **556** 599
[23] Baillard X, Gauguet A, Bize S, Lemonde P, Laurent P, Clairon A and Rosenbusch P 2006 *Opt. Commun.* **266** 609
[24] Gilowski M, Schubert C, Zaiser M, Herr W, Wübbena T, Wendrich T, Müller T, Rasel E M and Ertmer W 2007 *Opt. Commun.* **280** 443
[25] Wang B, Lv X K and Chen J B 2011 *Chin. Opt. Lett.* **9** 041402
[26] Xiao X and Yu F Q 2011 *SPIE Opt. Eng.* **50** 034201
[27] Ludeke R and Harris E P 1972 *Appl. Phys. Lett.* **20** 499